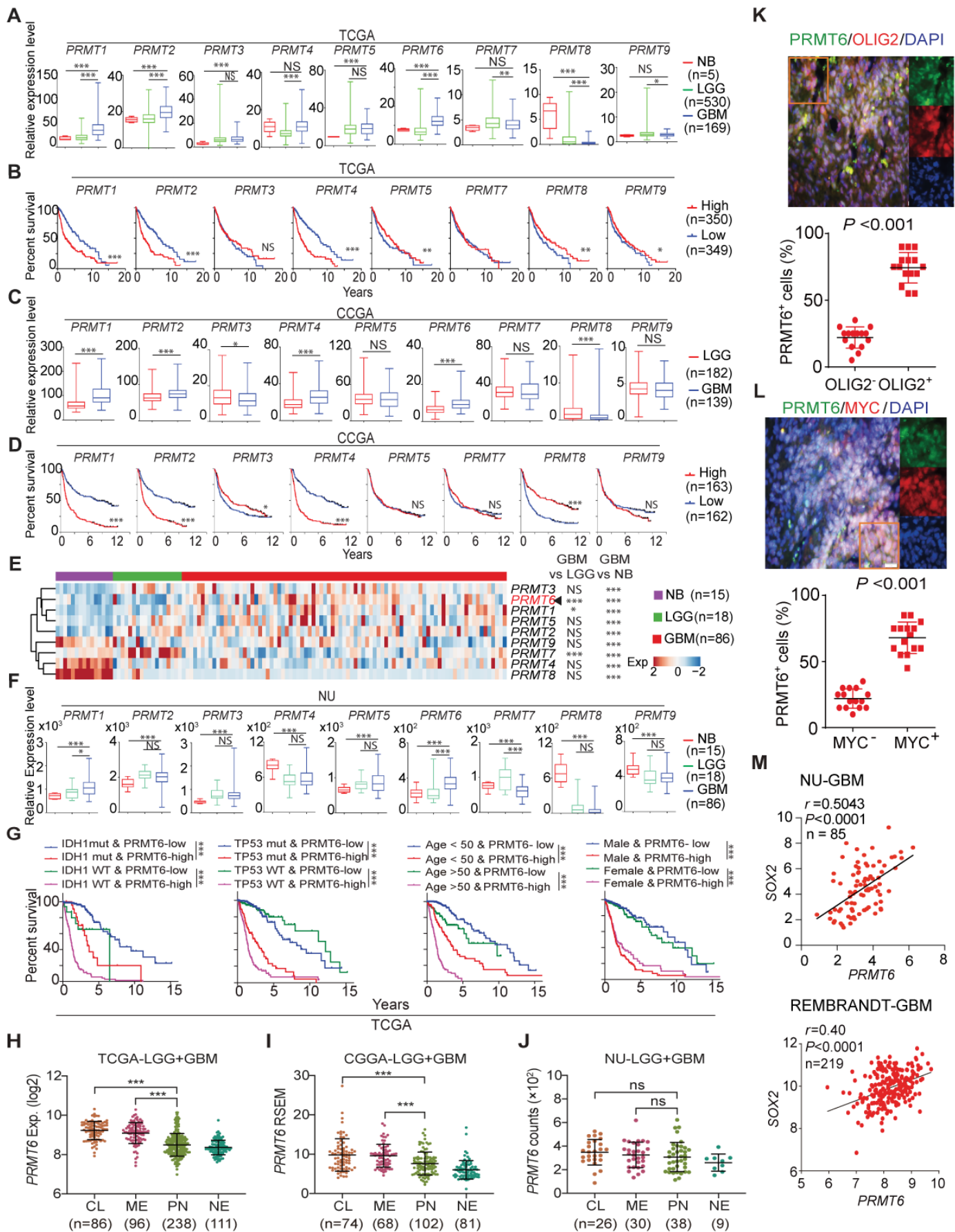


## **Supplemental Information**

### **PRMT6 Methylation of RCC1 Regulates Mitosis, Tumorigenicity, and Radiation Response of Glioblastoma Stem Cells**

Tianzhi Huang, Yongyong Yang, Xiao Song, Xuechao Wan, Bingli Wu, Namratha Sastry, Craig M. Horbinski, Chang Zeng, Deanna Tiek, Anshika Goenka, Fabao Liu, Cameron W. Brennan, John A. Kessler, Roger Stupp, Ichiro Nakano, Erik P. Sulman, Ryo Nishikawa, Charles David James, Wei Zhang, Wei Xu, Bo Hu, and Shi-Yuan Cheng

**Figure S1**



**Figure S1. Analyses of the expression of *PRMT* family members in normal brain, low-grade glioma (LGG), glioblastoma (GBM), and tumor prognosis. Related to Figure 1.**

(A, C, and F) Analyses of the TCGA datasets (A), CCGA (C) and Northwestern (NU) glioma cohort (F) for gene expressions of the *PRMT* family members between GBM, low-grade glioma (LGG), and normal brain (NB). Box plots indicate the median and upper and lower quartiles, with whiskers extending to the minimum and maximum range.

(B and D) Kaplan-Meier analyses of the TCGA (B) and CCGA (D) datasets for gene expressions of the *PRMT* family members.

(E) Heatmap of gene expressions of the *PRMT* family members in NB, LGG, and GBM specimens and statistical analysis of RNA-seq data of Northwestern (NU) glioma cohort for *PRMT* genes expression between GBM, LGG, and NB. One-way ANOVA followed by Dunnett's multiple comparisons test were used for determining the significance levels.

(G) Multivariate Kaplan-Meier analyses of the TCGA dataset for *PRMT6* expression versus status of *IDH1* and *TP53*, and age, and gender.

(H-J) Comparison of *PRMT6* expression levels among GBM MES, PN, CL, or NE subtypes in indicated datasets.

(K and L) Immunofluorescent staining (IF) of *PRMT6* (green), *OLIG2* (K, red) or *MYC* (L, red), and DAPI (blue for nuclei). Left: images of GBM (n = 5). Right: percentage (%) of *PRMT6*<sup>+</sup> cells among *OLIG2*<sup>+</sup> vs *OLIG2*<sup>-</sup> cells (K), or *MYC*<sup>+</sup> vs *MYC*<sup>-</sup> cells (L). Scale bar, 50  $\mu$ m. Lines,  $\pm$ SEM. Data are representative of two independent experiments with similar results.

(M) Pearson correlation between *PRMT6* and *SOX2* mRNA expression in the NU (left) and REMBRANDT (right) GBM datasets.

\*,  $p < 0.05$ ; \*\*,  $p < 0.01$ ; \*\*\*,  $p < 0.001$ ; NS, no significance.

**Figure S2**

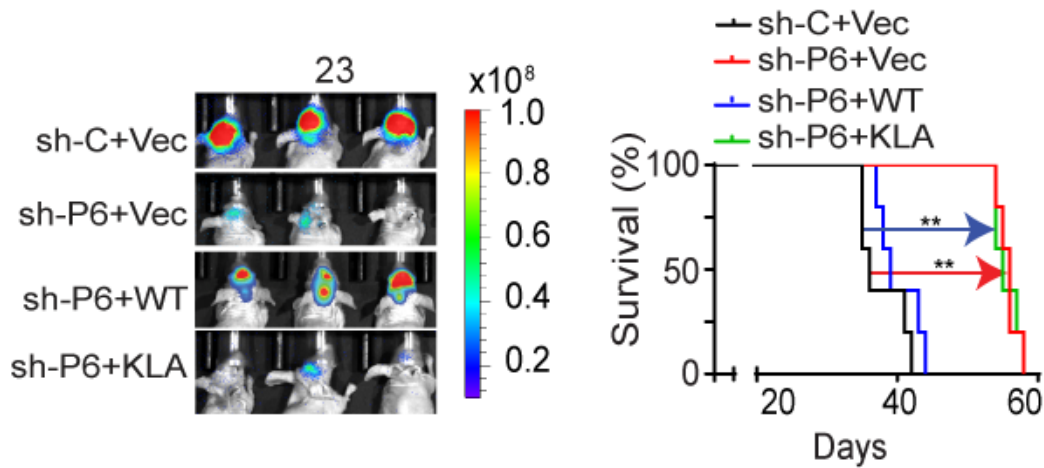


**Figure S2. PRMT6 activity is required for tumorigenicity of GSCs. Related to Figure 2.**

Left: *In vivo* bioluminescent imaging (BLI) of GBM brain xenografts derived from luciferase-expressing GSC23/*PRMT6* KD using a shRNA targeting 3' untranslated region of *PRMT6* mRNA, or a sh-C, and rescued with *PRMT6*-WT, enzymatically inactive KLA mutant or a vector control. Colored scale bar represents photons/s/cm<sup>2</sup>/steradian.

Right: Kaplan Meir analysis of mice received GSC23 with indicated modifications in the brain.

Data are representative of two independent experiments with similar results.

\*\* $p < 0.01$ .



**Figure S3. PRMT6 directly methylated RCC1 at R214 through protein association. Related to Figure 3.**

(A) IP-IP or IB for RAN activation, pS10H3, p21, and PRMT6 in GSC23/*PRMT6* KD and 576/*PRMT6* KO or controls.

(B) Cell-cycle profiles of GSCs with *PRMT6* KD, KO or controls.

(C, E) Sketches of WT and deletion mutants for *PRMT6* (C) and *RCC1* (E).

(D, F, and G) IP-IB and IB of HEK293T cells with indicated modifications for mapping of specific domains responsible for *PRMT6*-*RCC1* interaction.

(H) Left, representative IF images of interphase GSC576/*PRMT6* KO or sh-C cells with normal or abnormal nuclear morphology. Right, the frequency of indicated GSCs in interphase with abnormal nuclear morphology. n=200, interphase cells for each condition. Error bars,  $\pm$  SEM.

(I) Left: representative IF images of GSC576/*PRMT6* KO or sh-C cells with bipolar or supernumerary spindles during metaphase. Right: The frequency of indicated GSCs with supernumerary spindles was determined. n=200 metaphase cells for each condition. Error bars,  $\pm$  SEM.

(J, K) Cell proliferation (J) and sphere-forming frequency (K) of GSC576 cells with indicated modifications.

(L) The frequency of indicated GSC576 cells in interphase with abnormal nuclear morphology. n=200, interphase cells for each condition. Error bars,  $\pm$  SEM.

(M) The frequency of indicated GSC576 cells with supernumerary spindles. n=200 metaphase cells for each condition. Error bars,  $\pm$  SEM.

(N, Q) Box plots of the CCGA (N), NU glioma cohort (Q) for *RCC1* gene among NB, LGG, and GBM with indicated median.

(O, R) Kaplan-Meier analyses of the CCGA LGG+GBM (O), NU GBM (R) dataset for *RCC1* expression. Data in R only included GBM since survival data of NU LGG samples are not available.

(P, S) Pearson correlation between *PRMT6* and *RCC1* expression in the CCGA (P), NU glioma cohort (S) LGG+GBM dataset. Scale in both axis: log<sub>2</sub> (TPM).

(T) *In vivo* methylation assays of *RCC1* by recombinant Halo-PRMT 1-8 proteins. The resultant products were immunoprecipitated of HEK293T cells with indicated modifications using an anti-Flag antibody and then analyzed by IB using an anti-aDMA antibody.

(U) IB for *RCC1*, *RCC1*me<sub>2</sub> in the peptide encoding AA 251-274 of *RCC1* (an aDMA 214, QGQLGRVPEL FAN**R (me<sub>2</sub>)**GGRQGL ERLL) or an unmodified peptide with AA 251-274 sequence of *RCC1* in GSC576 with or without *PRMT6* KO or *RCC1* KD using indicated antibodies.

(V) Representative images of immunohistochemistry (IHC) assays on a clinical GBM specimen using the rabbit anti-*RCC1* Rme<sub>2</sub>-specific (anti-*RCC1*me<sub>2</sub>) antibody in the absence (upper) or presence (lower) of a *RCC1* aDMA 214 peptide. Scale bars, 50  $\mu$ m.

(W) Identification of methylated R214 of the *in vitro* methylated His-*RCC1* protein using liquid chromatography coupled tandem mass spectrometry (LC-MS/MS).

In (A) and (U),  $\beta$ -actin was used as a loading control for IB and a negative control for IP RanBP1 assays. In (D), (F), (G), and (T), HA or Flag was used as loading controls for IP or IB.

Data are representative of two to three independent experiments with similar results. \*,  $p < 0.1$ ; \*\*,  $p < 0.01$ ; Scale bars in (H, I), 5  $\mu$ m; in (V), 50  $\mu$ m.

**Figure S4**

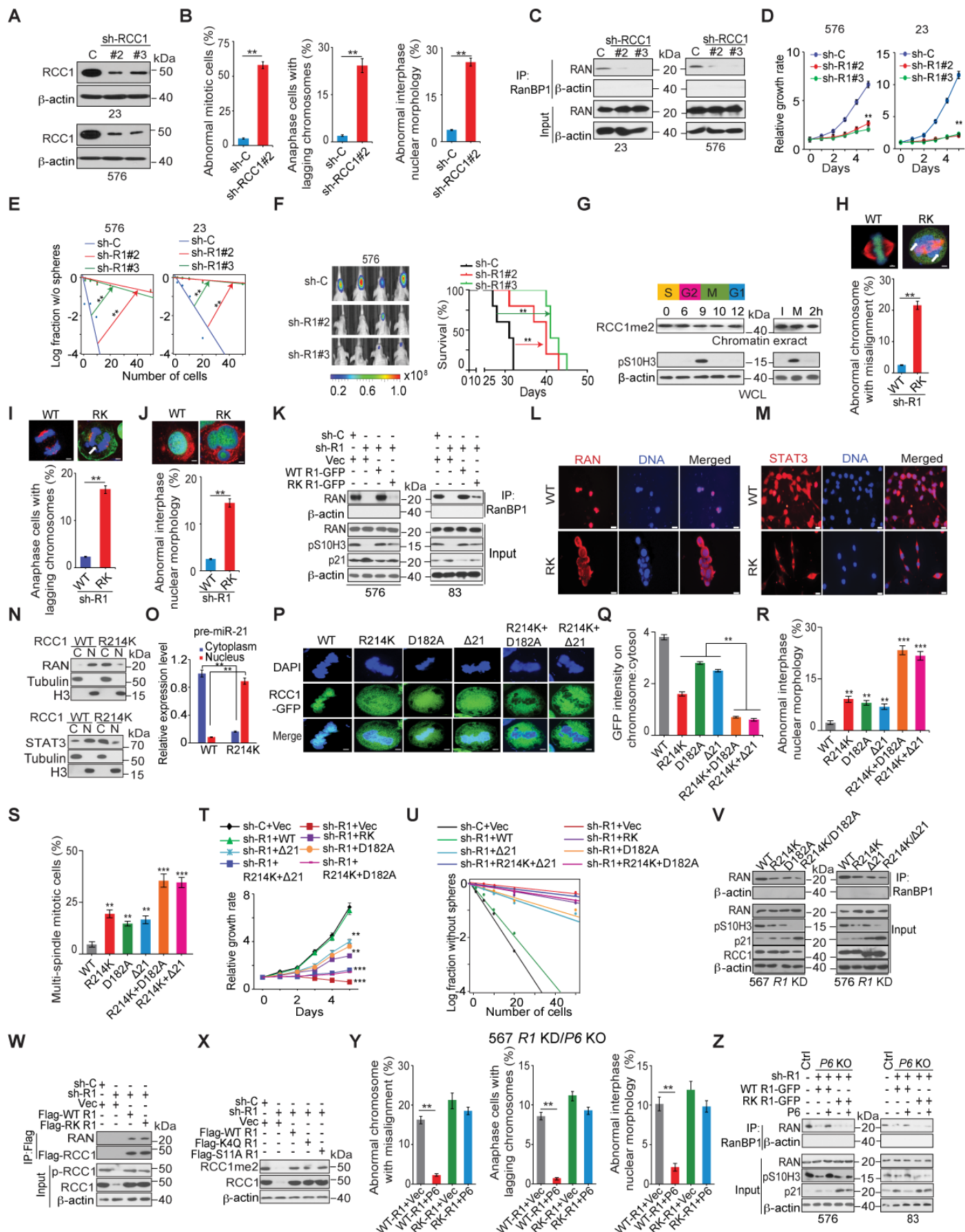


**Figure S4. Knockdown of *RCC1* and inhibition of *RCC1* methylation result in defects in cell mitosis, cell growth, self-renewal, and tumorigenicity of GSCs. Related to Figure 4.**

(A) IB for shRNA KD of *RCC1* in GSC23 and 576 cells.

(B) The frequency of GSC576/*RCC1* KD cells with abnormal mitotic phenotypes, lagging chromosome during anaphase, and abnormal interphase nuclear morphology. n=100 interphase or mitotic cells for each condition.

(C) IP-IB and IB for RAN activation in GSC23 and 576 cells with *RCC1* KD or a control.

(D and E), cell proliferation (D), sphere-forming frequency (E) of GSC23 and 576 with *RCC1* KD or a control.

(F) Left, *in vivo* BLI of GBM brain xenografts derived from the luciferase-labeled GSC576 with or without *RCC1* KD. Right, Kaplan-Meier analyses of mice received GSC576 with indicated modifications (n = 5).

(G) IB for *RCC1*m2 and pS10H3 in chromatin extracts (upper) or cell lysates (lower) of GSC576 cells that were synchronized by thymidine double block (2 mM) then released for the indicated periods of time (left) or for 6 h, followed by nocodazole (20 ng/ml) treatment for 12 h (right), with or without removal of nocodazole for 2 h thereafter.

(H) Upper, representative IF images of GSC576/*RCC1* KD cells rescued with *RCC1* WT or R214K mutant for chromosomal alignments. Lower, the frequency of abnormal chromosomes with misalignment in GSC576 cells with indicated modifications. n=50 mitotic cells for each condition.

(I) Upper, representative IF images of anaphase GSC576/*RCC1* KD cells rescued with *RCC1*-GFP WT or R214K (RK). Lower: the frequency of anaphase cells with lagging chromosomes. n=50 anaphase cells for each condition.

(J) Upper, representative images of interphase GSC576/*RCC1* KD cells rescued with *RCC1*-GFP WT or R214K (RK). Lower, the frequency of indicated GSC576 cells with abnormal interphase nuclear morphology. n=200 interphase cells for each condition.

(K) IP-IB for RAN activation, pS10H3, and p21 in GSC576/*RCC1* KD and 83/*RCC1* KD or control (sh-C) cells that were transduced with a vector, *RCC1*-GFP WT, or R214K (RK).

(L and M) Mislocalization of RAN (L) and STAT3 (M) to the cytoplasm on R214K cells. GSC576/*RCC1* KD cells rescued with *RCC1*-GFP WT or R214K (RK) were fixed and stained with antibodies against Ran (L) or Stat3 (M), and DAPI. GSCs were treated with 20 ng/ml IL-6 for 30 min to induce Stat3 activation. Scale bar, 20  $\mu$ m.

(N) IB. Levels of RAN (upper) and STAT3 (lower) in cytoplasm (C) and the nucleus (N) were examined in GSC576/*RCC1* KD cells rescued with *RCC1*-GFP WT or R214K (RK). Tubulin, control for cytoplasmic protein; Histone H3, control for nuclear protein. GSCs were treated with 20 ng/ml IL-6 for 30 min to induce Stat3 activation.

(O) qRT-PCR detection of precursor miR-21 expression in cytoplasmic and nuclear fractionations.

(P) representative IF images of GFP (green) or DAPI (blue) for mitotic GSC576/*RCC1* KD cells rescued with *RCC1*-GFP WT or indicated mutant(s).

(Q) Ratios of relative fluorescence intensity of *RCC1* at chromosome versus centrosome (chromosomal:cytosolic GFP) and frequencies of indicated defects in mitotic and interphase in GSC576/*RCC1* KD cells rescued with *RCC1*-GFP WT, or indicated mutant(s). Data analyzed by two-tailed independent t tests. n=50 mitotic cells for each condition.

(R) The frequency of indicated GSC576 cells in interphase with abnormal nuclear morphology. n=200, interphase cells for each condition. Error bars,  $\pm$  SEM.

(S) The frequency of indicated GSC576 cells with supernumerary spindles. n=200 metaphase cells for each condition. Error bars,  $\pm$  SEM.

(T, U) Cell proliferation (T) and sphere-forming frequency (U) of GSC576 cells with indicated modifications.

(V) IP-IB and IB for RAN activation, pS10H3, and p21 in GSC576 cells with indicated modifications.

(W) IP-IB and IB for RAN, p-*RCC1*, and *RCC1* in GSC576 cells with indicated modifications.

(X) IP-IB and IB for RCC1me2 and RCC1 in GSC576 cells with indicated modifications.

(Y) The frequencies of abnormal chromosome with lagging misalignment, lagging chromosome during anaphase, and abnormal interphase nuclear morphology in GSC576/*RCC1* (*R1*) KD + *PRMT6* (*P6*) KO cells with indicated modifications. n=100 interphase or mitotic cells for each condition.

(Z) IP-IB or IB for RAN activation, pS10H3, and p21 in GSC576/*P6* KO and 83/*P6* KO or control (sh-C) cells that were co-expressed a shRNA for *RCC1* with a *RCC1*-GFP WT, R214K (RK) or *PRMT6* (*P6*).

In (A), (C), (G), (K), (V), (W), (X), and (Z),  $\beta$ -actin was used as a loading control for IB or and a negative control for IP RanBP1 assays.

In (B), (H-J), (O), (Q-T), and (Y), error bars,  $\pm$  SEM. Scale bars in (H, I, J, and P), 5  $\mu$ m.

\*,  $p < 0.05$ ; \*\*,  $p < 0.01$ ; \*\*\*,  $p < 0.001$ ;

Data are representative of two to three independent experiments with similar results.

Figure S5

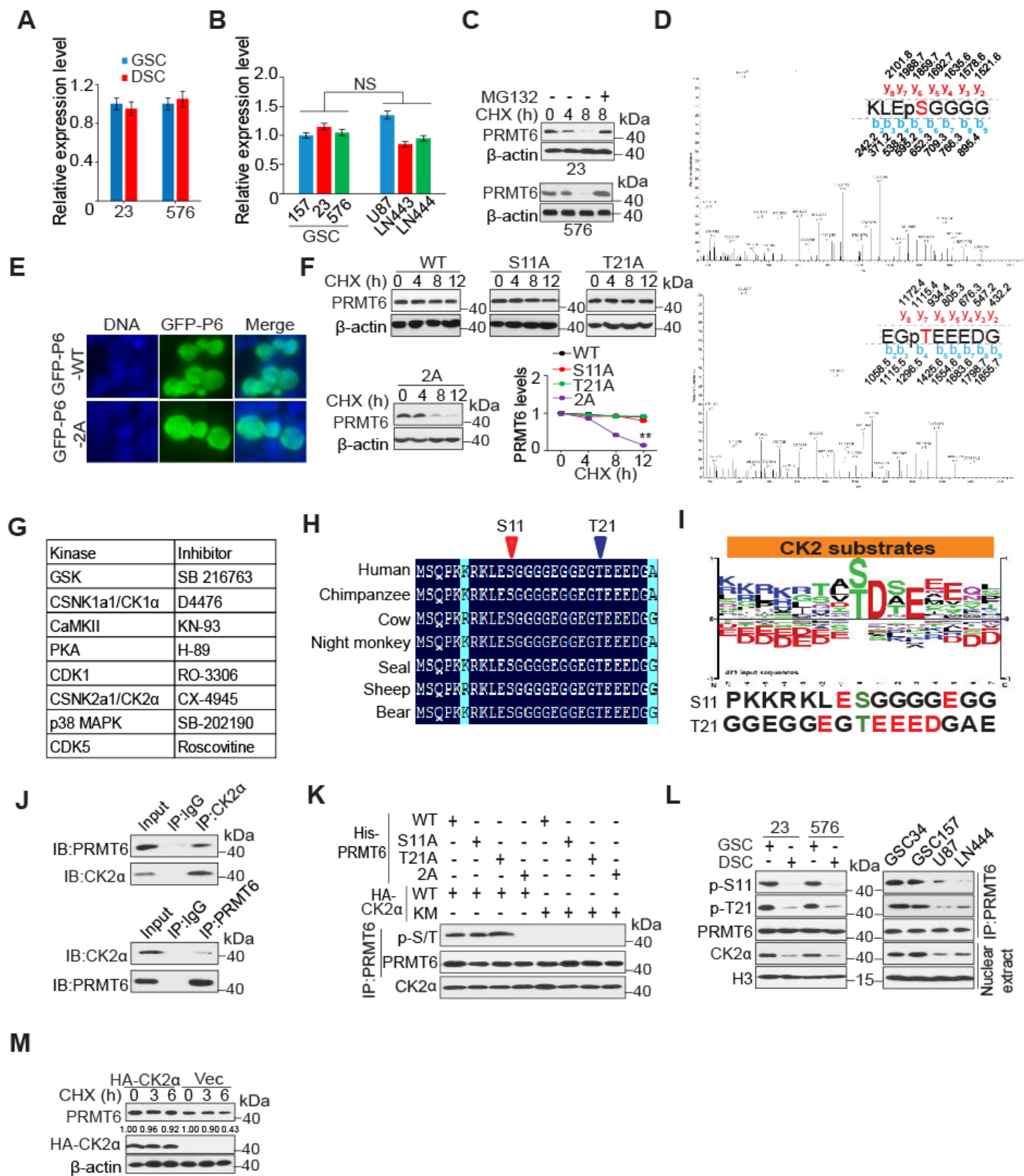


**Figure S5. CK2 $\alpha$  Phosphorylation of PRMT6 stabilized PRMT6 proteins through deubiquitylation. Related to Figure 5.**

(A) and (B), quantitative real-time PCR (qPCR) for mRNA levels of *PRMT6* in GSC23 and 576 and their corresponding differentiated glioma cells (A), indicated GSCs and established GBM cell lines (B). Data were normalized to that in GSC23 (A) or GSC157 (B). Error bars,  $\pm$  SEM., n=three independent experiments, two-tailed Student's t-test. ACTB was used as an internal control; NS, no significance.

(C) IB for PRMT6 protein in GSC23 and 576. GSC23 and 576 were treated with cycloheximide (CHX) with or without the proteasome inhibitor MG132 for the indicated times.

(D) Mass-spectrometric analysis of PRMT6 p-S11 (upper) and p-T21 (lower) for protein samples that were immunoprecipitated by an anti-Flag antibody from GSC576 cells that expressed exogenous HA-CK2 $\alpha$  proteins.

(E) Representative IF images of GFP (green) or DAPI (blue) for HEK293T/*PRMT6* KO cells that were transduced with an EGFP-*PRMT6* WT or 2A mutant.

(F) IB for PRMT6 in HEK293T/*PRMT6* KO cells that were transduced with a Flag-*PRMT6* WT, S11A, T21A or 2A mutant, and then treated with CHX for the indicated times. Right, quantification of the intensity of *PRMT6* in the IB blots in the right.

(G) A list for inhibitors that inhibit the indicated kinase. These inhibitors were used in the experiments shown in Figure 5E.

(H) Amino acid sequences around serine 11 and threonine 21 residue of PRMT6 protein across different species. Arrows at the top, S11 and T21 residues that are conserved across species.

(I) Sequence alignment of the conserved phosphorylation motif of CK2 $\alpha$  on its substrates (<https://www.cellsignal.com/products/proteomic-analysis-products/phospho-ck2-substrate-motif-s-t-dxe-kit/12170>), and amino acid (AA) sequence surrounding phosphorylated S11 and T21 residues of PRMT6 protein.

(J) IP-IB and IB for endogenous PRMT6 and CK2 $\alpha$  in GSC576 with indicated antibodies.

(K) *In vitro* kinase assays for p-S/T of PRMT6 in HEK293T cells co-expressed HA-CK2 $\alpha$ -WT, or K68M mutant with His-*PRMT6* WT, S11A, T21A or 2A mutant.

(L) IP-IB and IB for p-S11, p-T21 of PRMT6, PRMT6 and CK2 $\alpha$  in GSC23 and 576 cells with or without differentiation (left), in GSC34, 157, GBM U87 and LN444 cells (right). Nuclear extract from the indicated cells were used for IP and IB analyses.

(M) IB for PRMT6 in GSC576 cells that were transduced with HA-CK2 $\alpha$  and then treated with CHX at indicated times. Numerical numbers underneath were quantification of intensity of PRMT6 detected in the IB blot.

In (C), (F), and (M),  $\beta$ -Actin was used as a loading control.

In (K), HA for HA-CK2 $\alpha$  was used as a loading control.

In (L), H3 was used as a loading control.

In (A), (B), and (F), error bars,  $\pm$  SEM, n=3 independent experiments, two-tailed Student's t-test, \*\*,  $p < 0.01$

Data are representative of two to three independent experiments with similar results.

**Figure S6**

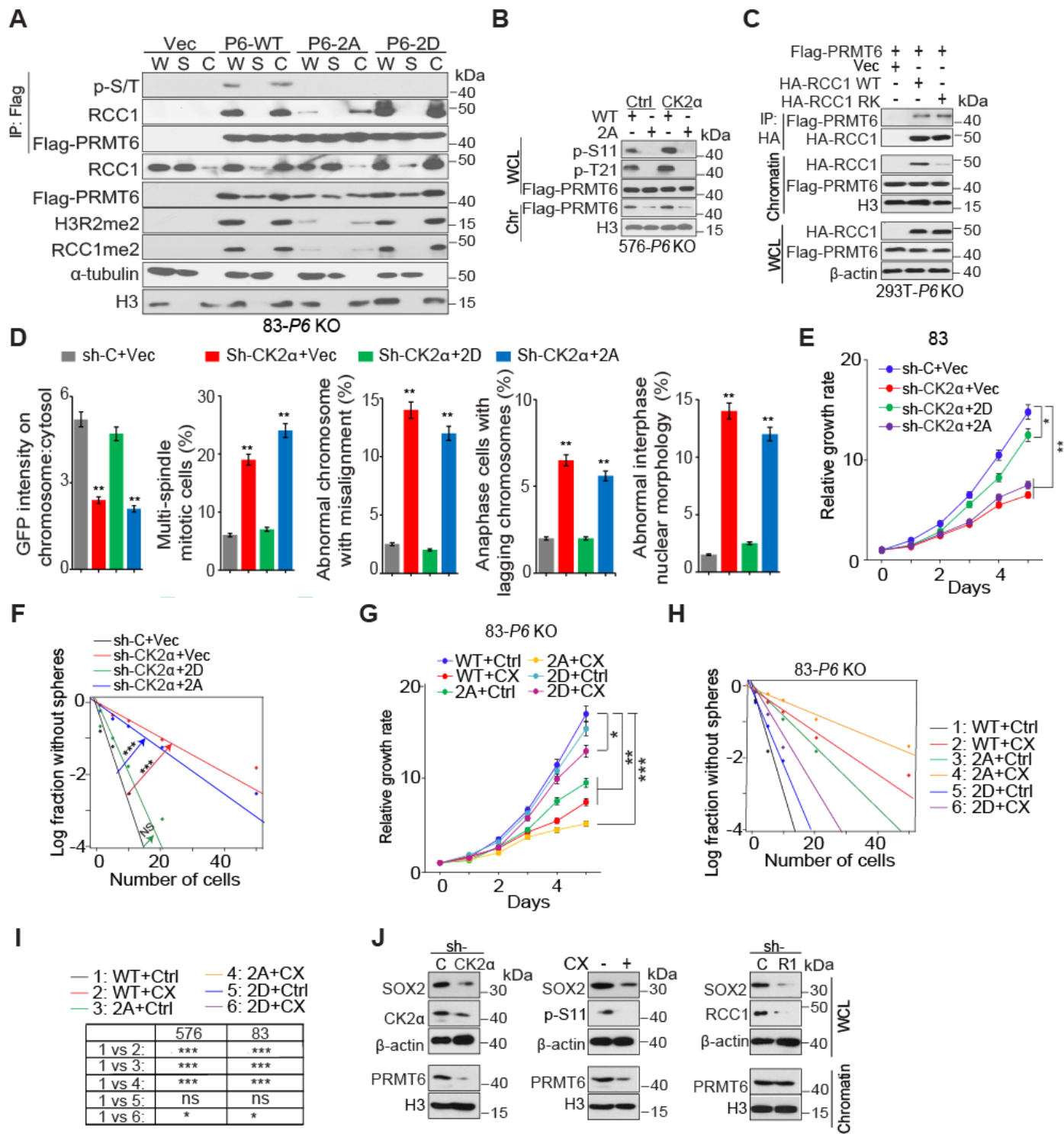


**Figure S6. CK2 $\alpha$  phosphorylation of PRMT6 promotes cell mitosis and tumorigenicity of GSCs. Related to Figure 6.**

(A) IP-IB and IB. Biochemical fractionation of GSC83 *PRMT6* KO cells expressing Flag-*PRMT6* WT, 2A, 2D mutant, or a control vector. Whole-cell (W), soluble (S), and chromatin (C) fractions were analyzed for with indicated antibodies. Tubulin was detected mainly in the soluble fraction. Histone H3 was primarily detected in the chromatin fraction.

(B) IP-IB and IB of whole cell lysates (WCL) and chromatin fractions (Chr) for PRMT6 association with chromatin in GSC 576/*PRMT6* (P6) KO cells co-expressing Flag-*PRMT6* WT, or 2A, with a HA-CK2 $\alpha$  WT or a control vector. H3 was used as a chromatin loading control.

(C) IP-IB and IB of cell lysates and chromatin fractions for RCC1 association with PRMT6 and chromatin in HEK293T/*PRMT6* KO cells that co-expressed Flag-*PRMT6*, or a vector with a HA-RCC1 WT or R214K mutant and then treated with MG132 for 6 h.

(D) Ratios of relative fluorescence intensity of RCC1 at chromosome versus centrosome (chromosomal:cytosolic GFP) and frequencies of indicated defects in mitotic and interphase GSC83 cells with indicated modifications. Data were analyzed by two-tailed independent t-tests. n=100 interphase or mitotic cells for each condition. Error bars,  $\pm$  SEM.

(E and F), Cell proliferation (E) or sphere-forming frequency (F) of GSC83 with indicated modifications.

(G and H) Cell proliferation (G) or sphere-forming frequency (H) of GSC83/*PRMT6* KO cells reconstituted with Flag-*PRMT6* WT, 2A, or 2D mutant with or without CX-4945 treatment.

(I) Differences in sphere forming frequency among GSC576 and 83 cells with indicated modifications.

(J) IP-IB and IB of whole cell lysates (WCL) and chromatin fractions (Chr) for PRMT6 association with chromatin in GSC83 cells with indicated modification or treatment.

In (C) and (J),  $\beta$ -actin and H3 were used as WCL and chromatin loading controls, respectively .

Data in bar plots, and line graphs are means  $\pm$  SEM. \*,  $p < 0.05$ ; \*\*,  $p < 0.01$ ; \*\*\*,  $p < 0.01$ ;

Data are representative of two to three independent experiments with similar results.

**Figure S7**

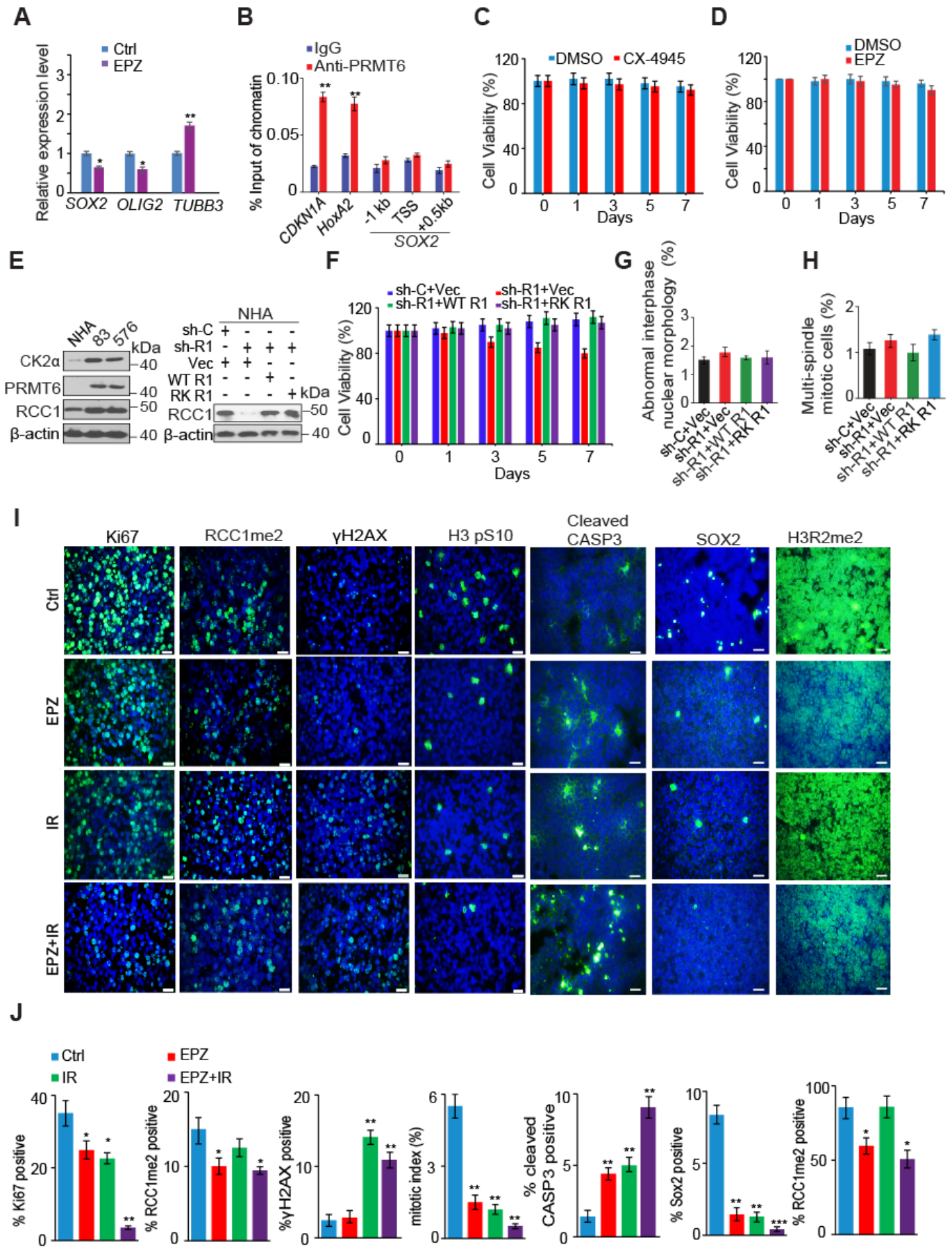


**Figure S7. Targeting PRMT6 attenuates GSC self-renewal, and enhances inhibitory effects of radiation therapy (RT) on GSC tumorigenicity. Related to Figure 7.**

(A) qPCR for mRNA levels of *SOX2*, *OLIG2*, and *TUBB3* gene expression in GSC23 with or without 20  $\mu$ M EPZ020411 treatment. Values were normalized to that in control group. ACTB was used as an internal control.

(B) GSC83 were harvested and subjected to ChIP analysis using antibodies against PRMT6 and a corresponding rabbit IgG control. Immunoprecipitated DNA was analyzed in triplicates by qPCR with primers spanning the indicated regions of the *SOX2* gene locus. Known gene targets of PRMT6, *CDKN1A* and *HOXA2*, were used as the positive controls.

(C and D) Cell viability for normal human astrocyte (NHA) cells treated with 5  $\mu$ M CX-4945 (C), or 20  $\mu$ M EPZ020411 (D) at indicated times.

(E) IB for CK2 $\alpha$ , PRMT6, and RCC1 in NHA, GSC576 and 83 cells (left), and IB for RCC1 in NHA cells with indicated modifications (right).  $\beta$ -actin was used as a loading control.

(F) Cell viability for NHA cells with indicated modifications.

(G) The frequency of indicated NHA cells in interphase with abnormal nuclear morphology. n=200, interphase cells for each condition. Error bars,  $\pm$  SEM.

(H) The frequency of indicated NHA cells with supernumerary spindles. n=200 metaphase cells for each condition. Error bars,  $\pm$  SEM.

(I) IF staining for Ki-67, RCC1me2,  $\gamma$ H2AX, H3pS10, cleaved caspase 3, *SOX2*, and H3R2me2 expression in brain sections with GSC23 brain tumor xenografts with indicated treatments. Scale bars, 20  $\mu$ M.

(J) Quantification of IF data in (I).

Data in the bar plots are means  $\pm$  SEM. \*,  $p < 0.05$ ; \*\*,  $p < 0.01$ , \*\*\*,  $p < 0.001$ .

Data are representative of two to three independent experiments with similar results.

**Figure S8**

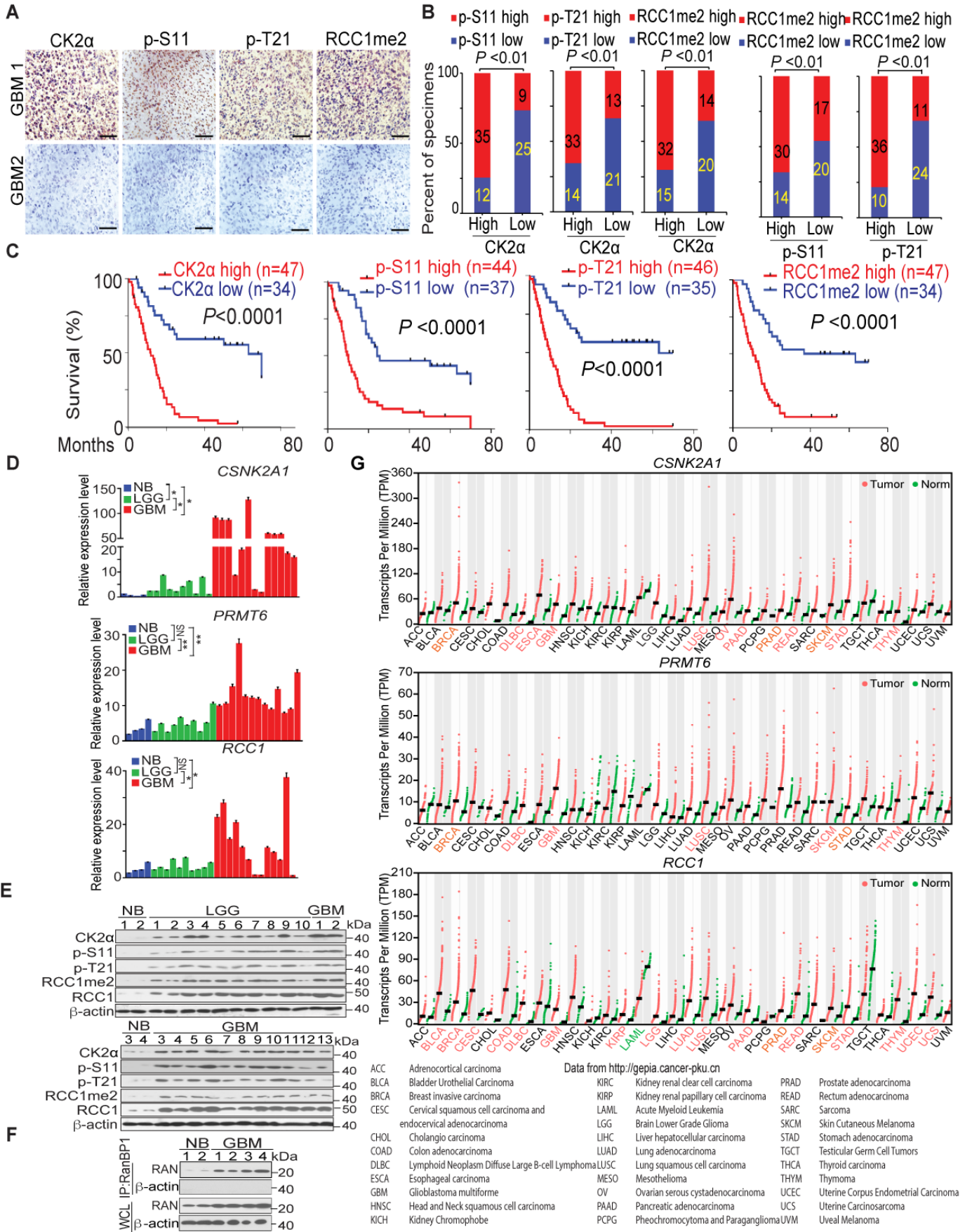


**Figure S8. Correlative Expressions of CK2 $\alpha$ , p-S11-PRMT6, p-T21-PRMT6, and RCC1me2 Are Prognostic Indicators for Clinical GBM. Related to Figure 7.**

(A) Representative images of IHC staining of CK2 $\alpha$ , p-S11-PRMT6, p-T21-PRMT6, and RCC1me2 in clinical GBM samples. Scale bars, 50  $\mu$ m.

(B) Correlations analyses of IHC data of GBM in (A). Statistical significance was determined by the  $\chi^2$  test. A total of 81 GBM tumor specimens were analyzed.

(C) Kaplan-Meier analyses for GBM tumors in (A). A total of 81 GBM tumor specimens were analyzed.

(D) qPCR for mRNA levels of *CSNK2A1*, *PRMT6*, and *RCC1* genes in NB, LGG, and GBM of the NU glioma cohort that was analyzed in Figure 1F.

(E) IB for CK2 $\alpha$ , p-S11-PRMT6, p-T21-PRMT6, PRMT6, RCC1me2, and RCC1 in NB, LGG, and GBM of the NU glioma cohort.

(F) IP-IB and IB for Ran activation (RanBP1) in NB, and GBM of the NU glioma cohort.

(G) Gene expression analysis for *CSNK2A1*, *PRMT6*, and *RCC1* between various human cancers (TCGA) and corresponding normal tissues (GTEx). Data was extracted from GEPIA (<http://gepia.cancer-pku.cn>). Tumor types in which genes were differentially expressed at 2-fold cutoff with q-value less than 0.01 were highlighted in red (upregulated in tumor) or green (downregulated in tumor).

In (E) and (F),  $\beta$ -actin was used as a loading control.

Data in the bar plots are means  $\pm$  SEM. \*,  $p < 0.05$ ; \*\*,  $p < 0.01$ , NS, no significance.

Data are representative of two to three independent experiments with similar results.